

ChemFit: A concurrent framework for model parametrization

Moritz Sallermann,^{†,‡} Amrita Goswami,^{†,‡} Hannes Jónsson,[†] Elvar Ö. Jónsson,^{*,†}
and Jorge R. Espinosa^{*,‡,¶,§,||}

[†]*Science Institute and Faculty of Physical Sciences, University of Iceland, VR-III, 107 Reykjavík, Iceland*

[‡]*Departamento de Química Física, Facultad de Ciencias Químicas, Universidad Complutense de Madrid, 28040 Madrid, Spain.*

[¶]*Yusuf Hamied Department of Chemistry, University of Cambridge Lensfield Road, Cambridge CB2 1EW, United Kingdom*

[§]*Phasica Biosciences S.L, Calle Velázquez, 27, 28001 Madrid, Spain*

^{||}*Multidisciplinary Institute, University Complutense of Madrid, Paseo Juan XXIII, 1, Madrid 28040, Spain*

E-mail: elvarorn@hi.is; jorgerene@ucm.es

Abstract

Parameter optimization in computational chemistry and physics often involves objective functions that are expensive to evaluate, noisy, non-differentiable, or composed of heterogeneous contributions originating from separate simulations. Gradient-free and black box optimization algorithms are powerful tools which are particularly well-suited to solving such optimization problems. However, interfacing simulation engines and parameter optimization libraries can be cumbersome, especially if simulations are expensive and need to be run concurrently. Here, we introduce ChemFit, a flexible Python framework for the definition, composition, and massively concurrent evaluation of simulation-based objective functions, which is designed to operate in conjunction with these algorithms. This framework provides abstractions for heterogeneous objective terms, file-based and in-memory quantity evaluation, and explicit control over concurrency across both objective components and parameter guesses. We demonstrate the versatility of ChemFit for different applications such as: (i) determination of Lennard-Jones parameters for liquid Argon from experimental den-

sity data over a range in temperature and pressure, using molecular-dynamics simulations, and (ii) the parameterization of a polarizable force-field for H₂O against the structure of small ice clusters obtained from density functional theory calculations. These examples illustrate how ChemFit enables scalable, reproducible, and optimizer-agnostic parameter fitting.

1 Introduction

The calibration of model parameters through comparison with experimental or reference data from high-level calculations is an important task in computational chemistry, physics, and related theoretical fields. Archetypal examples include the fitting of interatomic potentials and force-fields,^{1–10} the parameterization of coarse-grained models,^{11–17} and the optimization of phenomenological models used in geophysics and materials science.^{18,19} In many such applications, the evaluation of a single objective-function value requires the execution of one or more computationally intensive simulations, such as molecular dynamics (MD) and density functional theory (DFT).

These objective functions frequently exhibit characteristics that challenge traditional optimization approaches: they may be noisy due to finite sampling, non-differentiable due to discrete events or phase transitions, and composed of many heterogeneous contributions associated with independent data points or physical conditions.^{20,21} As a result, gradient-based optimization methods are often inapplicable, while grid-based parameter sweeps scale exponentially with dimensionality and rapidly become computationally prohibitive.²²

Gradient-free and black-box optimization methods, including evolutionary strategies,^{23,24} stochastic search,^{25,26} and Bayesian optimization,^{27–32} offer a powerful alternative.^{22,33} These approaches treat the objective function as an opaque mapping from parameters to scalar loss values and have found widespread use in fields ranging from hyperparameter optimization in machine-learning^{32,34,35} to experimental design and control.^{36,37} While, arguably, these algorithms are mature and ready-to-use, particularly for machine-learning,^{34,38} their application in the context of computational physics and chemistry is complicated by the need to orchestrate large numbers of concurrent, heterogeneous simulations. In addition, it is necessary to parse output data, aggregate results across many independent terms, and exploit concurrency at multiple levels to efficiently utilize available computational resources.

In this work, we introduce ChemFit, a framework designed to address this modeling gap. ChemFit focuses explicitly on the definition and execution of complex objective functions arising in simulation-based parameter fitting, thereby enabling the practical application of gradient-free optimization methods to large and realistic scientific problems. We illustrate the capabilities of our framework through two representative case studies:

1. Estimation of the Lennard-Jones model parameters for liquid Argon through molecular dynamics simulations, by fitting to available experimental data.
2. Parameterization of a polarizable water model using water clusters geometries obtained from DFT calculations as a reference.

2 Methods

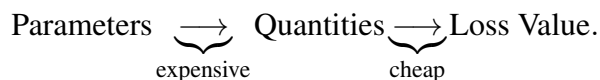
2.1 Software Design

An objective function is any kind of function that maps a set of input parameters to a single scalar value — the loss. The purpose of optimization algorithms is to find parameters, which minimize this loss value.

ChemFit splits the computation of the loss value into two steps:

1. The computation of intermediate *quantities* via explicit simulations. For instance these may be energies, densities or any observable obtained from computationally expensive (molecular) simulations, while the *parameters* could be the model parameters of the force-field being parameterized.
2. The *loss* is computed by applying a function that maps from the quantities (and the parameters) to a single scalar value. As a rule of thumb, these quantities are expensive to compute, while the loss is cheap (if the quantities are known).

We can summarize this procedure as follows



This split decouples the execution of computationally expensive simulations from the exact quantity which drives the optimization, and enables the accumulation of by-products of the simulation (in meta-data) which do not directly influence the optimization. Further, it increases flexibility since, once the mapping of parameters to quantities has been established, the loss function can be interchanged easily.

ChemFit encodes this relationship in an abstract interface, called a *QuantityComputer*. Out of the box, the framework comes with three pre-defined *QuantityComputers*:

1. The *FileBasedQuantityComputer*, which can execute arbitrary executables and coordinates user-supplied parsers to generate the quantities.

2. The *SinglePointASEComputer*, which runs any "Calculator" defined within the atomic simulation environment (ASE)³⁹ on a reference atom configuration.
3. The *MinimizationASEComputer*, which relaxes a configuration, using ASE, to a local minimum before evaluating the quantities.

Furthermore, additionally arbitrary user-defined *QuantityComputers* can be easily added. Once a *QuantityComputer* is defined, it needs to be combined with a loss function, e.g. a simple root mean square deviation (RMSD) and the objective function is ready to use. Detailed explanations of how to use ChemFit can be found in the online documentation⁴⁰ and examples.⁴¹

2.2 Concurrency

Concurrency enters the optimization procedure in three different ways, described in the following sections: (i) Simulation engine parallelism, (ii) Objective function parallelism and (iii) Parameter trial parallelism.

Computational resources should be allocated to these modes in the order listed above, only moving to the next mode once the limitations of the current mode are reached. In other words, individual simulations should be parallelized up to the strong scaling limit, after which resources should then be used to parallelize the computation of the objective function of sample points, and so on.

2.2.1 Simulation engine parallelism

At the most basic level, most simulation codes, such as LAMMPS,⁴² GROMACS⁴³ or VASP,⁴⁴ are themselves able to utilize multiple threads and/or processes. If the "size" of the system is held constant, however, there is a soft upper limit up to which computational resources without suffering from significant diminishing returns—this limit is dictated by the strong scaling efficiency of the code in question.^{45,46}

2.2.2 Objective function parallelism

If the objective function entails computations for multiple sample points—for instance, say the ob-

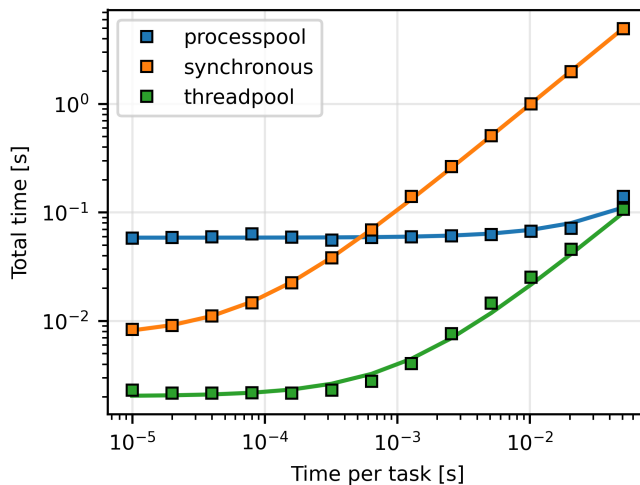


Figure 1: Total time taken to evaluate a combined objective function with ten individual terms (y-axis), versus the time it takes to evaluate each individual term (x-axis). Different colors correspond to different concurrency schemes. The solid lines serve as visual guides and are linear fits to the data points (evenly weighted in log-log space). The total number of available threads or processes, respectively, was 48.

jective function is a combined function of 100 points—the simulations for these points can be run in parallel (for a particular parameter trial set). In ChemFit this is achieved by defining a *CombinedObjectiveFunction* and parallelizing it either via the message passing interface (MPI) or a Python executor, such as the "processpool" and "threadpool" provided by the standard library, or third party libraries like "dask"⁴⁷. While objective function concurrency has excellent strong scaling efficiency, since all samples are independent, it is limited in two ways: (i) the wall-time can never be lower than the slowest sample point, which for extremely long simulations can severely limit the number of trial parameter sets tested, and (ii) the parallelism is limited by the number of sample points.

Fig 1 depicts the results of a benchmark comparing a threadpool and a processpool for objective function parallelism. The total time taken to evaluate a combined objective function with 96 individual terms is plotted on the y-axis, whereas the time required to evaluate each individual term of the combined objective function is shown on the x-axis. Forty-eight threads or processes, re-

spectively, were used for the benchmark. We observe that, once the evaluation of individual sample points takes more than approximately 1 ms, both avenues to parallelism are beneficial. Before that point, the serialization and communication overhead of the process pool, overshadows the benefits of parallelization. In general it is only necessary to use a process pool, when running pure Python code, which is unable to release the global interpreter lock (GIL). We should also remark that 1 ms constitutes an *extremely* low wall time for most simulation workloads we are aware of. In our experience, wall times ranging from several seconds to many hours are more typical. If individual samples can indeed be evaluated within a milli second, our recommendation would be to either batch the evaluation or to avoid using ChemFit and, most likely, Python altogether.

2.2.3 Parameter trial parallelism

Lastly, the objective function can be evaluated for multiple candidate parameter sets in parallel. This mode of concurrency has excellent strong scaling efficiency and, in contrast to simulation engine parallelism (Sec. 2.2) and objective function parallelism (Sec. 2.2.2), there is no practical limit to the amount of parallelism which can be leveraged in this way.

However, a significant drawback can be illustrated by considering that two trials in sequence are more valuable than two trials in parallel. This is because the second trial can use the result of the first trial to refine its guess—the generalization to multiple trials is obvious. On one hand, exploiting this mode of concurrency is a detail of the optimization algorithm—most black-box algorithms support it trivially via some variation of an “ask-and-tell” interface. On the other hand, objective functions that support correct parallel evaluations need to avoid so-called race conditions, occurring when multiple threads or processes access shared resources simultaneously leading to undefined behaviour. To avoid race conditions, ChemFit provides a unique *EvaluateContext per objective function evaluation*. This means one objective function can be evaluated in N threads or processes by instantiating N *EvaluateContexts*, which encapsulate the access to shared resources.

3 Applications & Examples

3.1 Re-discovering the Lennard-Jones parameters for liquid Argon

In this case study, we revisit a prototypical problem: liquid Argon modeled by the Lennard-Jones (LJ) potential,⁴⁸

$$U_{\text{LJ}}(r) = 4\epsilon \left[\left(\frac{\sigma}{r} \right)^{12} - \left(\frac{\sigma}{r} \right)^6 \right], \quad (1)$$

where r is the distance between two interacting Argon atoms, σ corresponds to the size of the atoms, and ϵ represents the interatomic binding energy. The attractive $1/r^6$ term corresponds to the London dispersion forces,^{49,50} derived from quantum mechanical perturbation theory and the repulsive term is phenomenological.⁵¹ Even though the success of the LJ potential in describing liquid Argon is likely due to a lucky coincidence^{52–54}, its popularity and extensive application to other systems make it a natural choice for an example such as the following.

We will determine the binding energy, ϵ , and the molecular diameter, σ by fitting to experimentally measured densities of liquid Argon in a range of 100.9 K to 143.1 K and pressures up to 680 atm obtained by Streett and Staveley⁵⁵. In total, these measurements encompass 139 independent data points. We intentionally choose initial parameters which are far away from the known literature values,^{56–59} and which do not even correspond to the liquid phase.⁶⁰ We use LAMMPS⁴² to generate the molecular dynamics (MD) trajectories. Given the fact that the optimization with ChemFit needs to evaluate a wide range of different ϵ and σ candidates, it is important to have a well-crafted and robust LAMMPS script. Details of the simulation setup for the LJ calculations can be found in Sec. S1.1 of the SI.

3.1.1 ChemFit setup

As depicted in Fig. 2, a *CombinedObjectiveFunction* is used to tie together individual terms expressed via the *FileBasedQuantityComputer* class, which handles the dispatch of individual

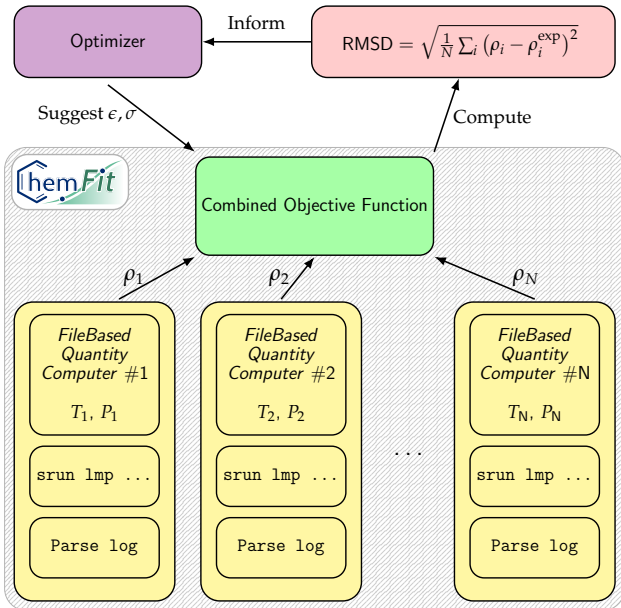


Figure 2: Flowchart depicting the use of ChemFit with LAMMPS to fit to the experimental Argon densities. For each experimental data point, a *FileBasedQuantityComputer* is created, which handles the creation of an appropriate LAMMPS input script, for each trial parameter set of σ and ϵ . The *FileBasedQuantityComputer* also uses an output parser to analyze the log files created by LAMMPS to obtain the averaged densities.

LAMMPS processes and the parsing of the output files. The number of terms is equal to the number of experimental data points (139). For the loss function, we use the root mean square deviation (RMSD) between the simulated densities (obtained as described in the simulation protocol section in Sec. 1.1 of the SI) and the experimental densities by Streett and Staveley⁵⁵

$$O(\epsilon, \sigma) = \sqrt{\frac{1}{N} \sum_{i=1}^N (\rho_i(\epsilon, \sigma) - \rho_i^{\text{exp}})^2}, \quad (2)$$

where N is the total number of data points (here, $N = 139$), ρ_i is the simulated density for temperature T_i and pressure P_i and ρ_i^{exp} is the experimentally measured density.

We ran ChemFit on a single cluster node with 128 cores. Per evaluation of a parameter set (ϵ , σ), which involves the computation of 139 densities, we used 64 cores. To evaluate each density for a given (ϵ , σ) we ran LAMMPS with a single

Table 1: Suggested LJ parameters, ϵ and σ , for liquid Argon from selected references in the literature and this work.

Source	ϵ [k_B]	σ [\AA]
Rahman (1964) ⁵⁶	120	3.4
Barker (1971) ⁵⁷	142.95	3.361
Rowley (1975) ⁵⁸	119.8	3.405
White (1999) ⁵⁹	125.7	3.345
This work	118.74	3.396

core. Thus, we evaluated two parameter sets concurrently at all times—saturating the entire node, thereby leveraging objective function parallelism (see also Sec. 2.2.2).

3.1.2 Results

In Fig. 3A, we show the phase space explored by the LJ system in one ChemFit run. The run starts from $\epsilon = 1$ kcal/mol $\approx 503 k_B$ and $\sigma = 1.5 \text{ \AA}$, and ends with parameters which are close to previously published results (see Tab. 1). As commonly used for LJ calculations, Fig. 3A is expressed in reduced units. The reduced density ρ_{red} is

$$\rho_{\text{red}} = \frac{n_{\text{atoms}}}{V} \sigma^3, \quad (3)$$

where ρ_{red} is the reduced density, n_{atoms} is the number of atoms, and V is the volume. The reduced temperature, T_{red} , is

$$T_{\text{red}} = \frac{k_B T}{\epsilon}, \quad (4)$$

where k_B is the Boltzmann constant and T is the temperature.

Fig. S1 in the SI depicts the agreement of the simulated densities using our optimal parameters with the 139 experimental density points. While the values agree very well, it is important to emphasize that other quantities of interest, to which the force-field has not been fitted to may be reproduced much less faithfully. Tab. 1 compares the final results of our optimization to previously reported ϵ and σ values (also shown in Fig. S2 in the SI). Our results are very similar to the results of Rahman⁵⁶ and Rowley et al.⁵⁸

Another point to consider is that, although the

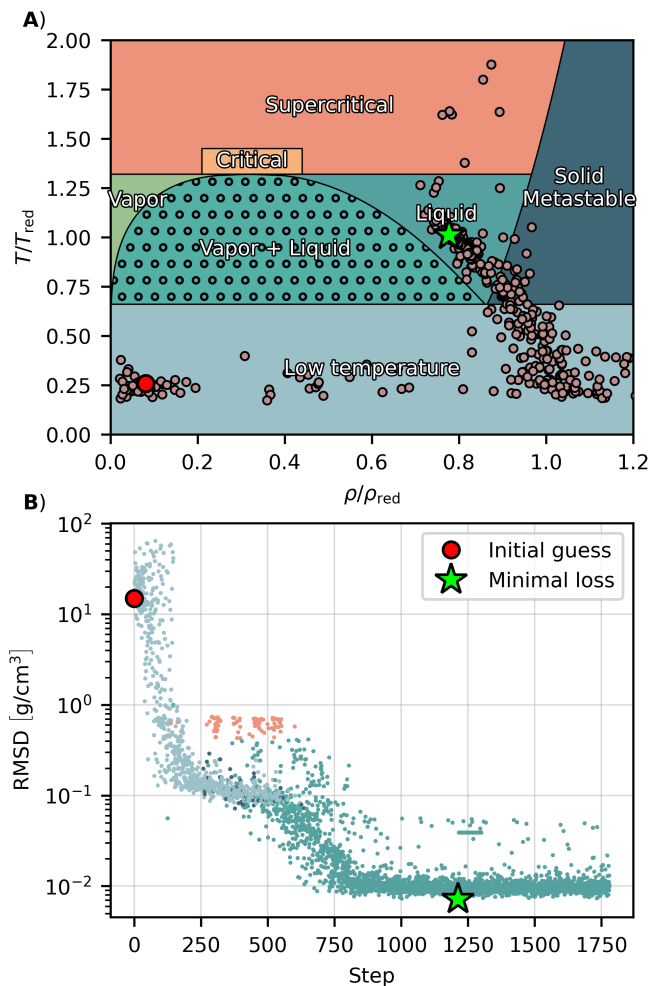


Figure 3: **A)** “Trajectory” (brown dots) of the optimization in the space of reduced density (x -axis) and reduced temperature (y -axis) for one of the 139 experimental measurements of liquid Argon by Streett and Staveley⁵⁵ at $p = 340.23$ atm, $T = 120.18$ K and with measured density of 1.32 g/cm³. The data is overlaid upon the phase-diagram of the Lennard-Jones system as per Stephan et al.⁶⁰ The initial guess is marked with a filled red circle and the point with minimal root-mean-square deviation (RMSD) over all 139 experimental points with a green star. **B)** RMSD versus optimization step. For each step two points were run in tandem, so that the total number of simulations corresponds to twice the number of steps. The points are colored according to the phase in which the majority of the 139 physical systems lie.

densities at different pressures and temperatures are often used as target properties in force-field parameterization,^{61,62} Méndez-Bermúdez et al.⁶³

recently showed that using the surface tension as a fitting parameter improves the simultaneous reproduction of the experimental phase behaviour and surface tension of liquid Argon. The densities are sufficient for our illustrative example, but multiple target properties could, in principle, be combined in ChemFit.

3.2 Parameterizing a polarizable force-field for H₂O

Next, we parametrize the flexible single-center-multipole-expansion (SCME) classical force field for H₂O^{10,64–67} to reproduce the geometry of small ice clusters, which locally minimize the energy obtained from density functional theory (DFT) with the BEEF-vdW functional⁶⁸ as implemented in VASP.⁴⁴ The clusters are composed of different isomers of dimers up to hexamers. In particular cyclic water hexamers have been found to be nearly iso-energetic,⁶⁹ making their geometries an interesting target property for parameterization.⁷⁰

In the SCME potential, the electrostatics of a water molecule are described by a static Cartesian multipole expansion ranging from dipole up to, and including, hexadecapole. Additionally, dipole-dipole, dipole-quadrupole and quadrupole-quadrupole polarizabilities are included giving rise to induced dipole and quadrupole moments¹⁰. We used the flexible variant of the SCME potential, called SCME/f, introduced by Jónsson et al.⁶⁴, which further implements a dependence of the static dipole and quadrupole moment on the geometry of the H₂O molecule (OH bond lengths and angle) balanced by an energy term favoring the equilibrium geometry described by the Partridge-Schwenke⁷¹ potential energy surface of the water monomer.

The full details of the formulation of the electrostatics in the SCME/f potential are best studied from dedicated references^{10,66,67}. Nonetheless, for the current example, we need to mention that, instead of using the bare Coulomb interactions, the SCME potential applies a Gaussian smearing type damping function⁷², which effectively screens the electrostatic interactions at short distances. The damping length is controlled by a free parameter τ_E , which among others, we will

optimize with ChemFit. A more detailed explanation of the electrostatic damping can be found in the SI. In addition to the electrostatic interactions, the SCME/f force field contains a dispersive interaction

$$E_{\text{Disp}} = \frac{1}{2} \sum_{ij} \left[\frac{C_6}{r_{ij}^6} g_6(r_{ij}) + \frac{C_8}{r_{ij}^8} g_8(r_{ij}) + \frac{C_{10}}{r_{ij}^{10}} g_{10}(r_{ij}) \right], \quad (5)$$

where the indices i and j label the *Oxygen* positions, r_{ij} is the distance between i and j ; C_6 , C_8 and C_{10} are constants quantifying the correlation between instantaneously induced moments due to fluctuating densities including e.g. dipole-dipole, dipole-quadrupole, dipole-octupole and quadrupole-quadrupole polarizabilities. Moreover, $g_n(r)$ is a short ranged damping function, following the Tang-Toennis form⁷³

$$g_n(r) = 1 - e^{-\tau_d r} \sum_{k=0}^n \frac{(\tau_d r)^k}{k!}, \quad (6)$$

where τ_d is another free parameter—the damping strength. In the original SCME/f, the coefficients C_6 to C_{10} were adopted from Hettema et al.⁷⁴ Lastly, the repulsive core contribution is given by a modified Born-Mayer potential⁶⁶

$$E_{\text{Rep}} = \frac{1}{2} \sum_{ij} A \left(\frac{r_{ij}}{L} \right)^B e^{C r_{ij}}, \quad (7)$$

where A , B , C are free parameters and $L = 1 \text{ \AA}$ is a constant introduced to simplify unit conversions.

3.2.1 ChemFit setup

Since the SCME/f potential is available as a "Calculator" in the atomic simulation environment (ASE)³⁹, we used the built-in *MinimizationASE* quantity computer, which minimizes the energy of an initial reference configuration and then computes certain quantities. In our objective function, the deviation of the minimized positions from the reference configuration is quantified via the root-mean-square-deviation (RMSD) of atomic positions *after* applying an optimal rotation and translation determined with the Kabsch algorithm^{75,76}.

A one-to-one correspondence between atoms in the reference configuration and in the minimized configuration is assumed. For the reference configurations we used the locally optimal configurations obtained from structure optimization from *ab initio* calculations (details of these simulations can be found in the SI). The loss function is simply the sum of the atom position RMSD values after applying the Kabsch rotation and translation.

In order to illustrate the optimization process, we optimize the eight parameters listed in Tab. 2 and start from initial values that are different from the reported literature values by Jónsson et al.⁶⁶

3.2.2 Results

In Fig. 4, we show the values of the RMSD, calculated using the Kabsch algorithm,^{75,76} of various water clusters obtained from an energy minimization with the SCME, using the initial (solid red line) and optimal parameters (solid green line). The RMSD constitutes the loss—lower values indicating a better agreement with the reference geometry.

The energies of the water clusters, computed with the SCME/f potential and using the optimal parameters (found solely by fitting to the geometry) agree well with those from DFT, as shown in Fig. 5. It is interesting that the structures of these water clusters correspond closely to the energies, although this could come at the cost of other desirable features in the potential, for instance, the dimer binding curves or cohesive energies of ice crystals.

The most significant differences between the optimal parameters found with ChemFit and, both, the initial parameters as well as the parameters by Jónsson et al.⁶⁶ seem to stem from the short range repulsion: the parameters A and B in Eq. (7) are quite different. Of course – considering the small size and rather specific nature of the reference data set – this present case study is in no way a proposition of a new potential parametrization. However, a follow-up investigation of how other properties are affected might be insightful.

Table 2: Results of parameter optimization of the SCME potential in atomic units – E_h denotes one Hartree of energy and a_0 is the Bohr radius. The initial values, the values after optimization and the literature values according to Jónsson et al.⁶⁶ are listed.

Parameter	Initial value	Optimal value	Jónsson et al. ⁶⁶
τ_E [a_0]	2.0	2.012	2.087
τ_D [a_0^{-1}]	4.7	4.21	4.0
C_6 [$E_h a_0^6$]	46.44	45.85	46.44
C_8 [$E_h a_0^8$]	1141.7	1141.75	1141.7
C_{10} [$E_h a_0^{10}$]	33441	33441	33441
A [E_h]	353.57	1327.09	299.493
B []	-0.146	-1.14	-0.5515
C [a_0^{-1}]	-2.002	-1.986	-1.836

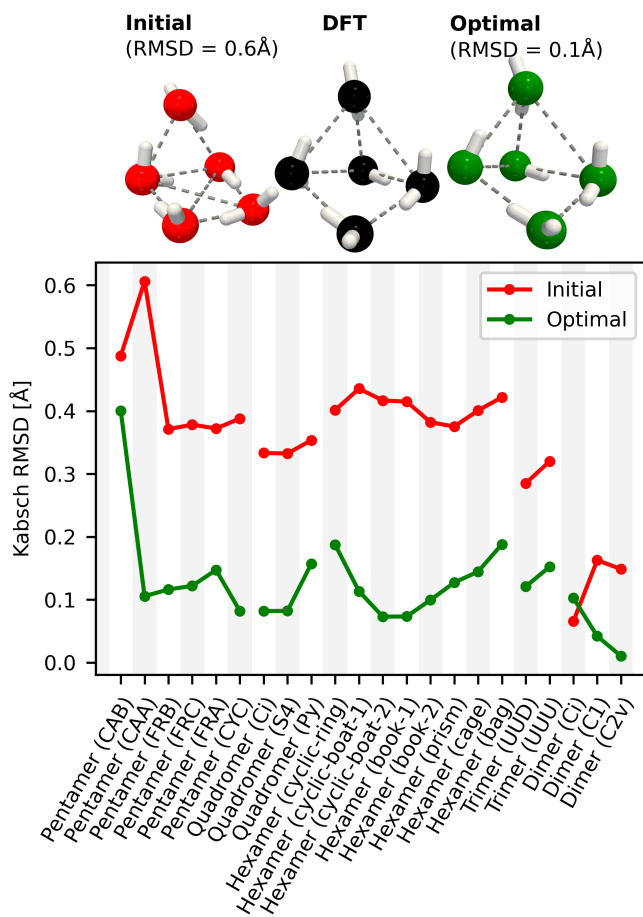


Figure 4: **Bottom:** Results for the RMSD from the Kabsch algorithm^{75,76} for the initial and optimal geometries, compared to reference geometries from DFT. **Top:** Snapshots of the initial, reference and optimal geometry of the water cage pentamer CAA. Dashed grey lines are a guide for the eye, connecting oxygen atoms that are less than 3.5 Å apart.

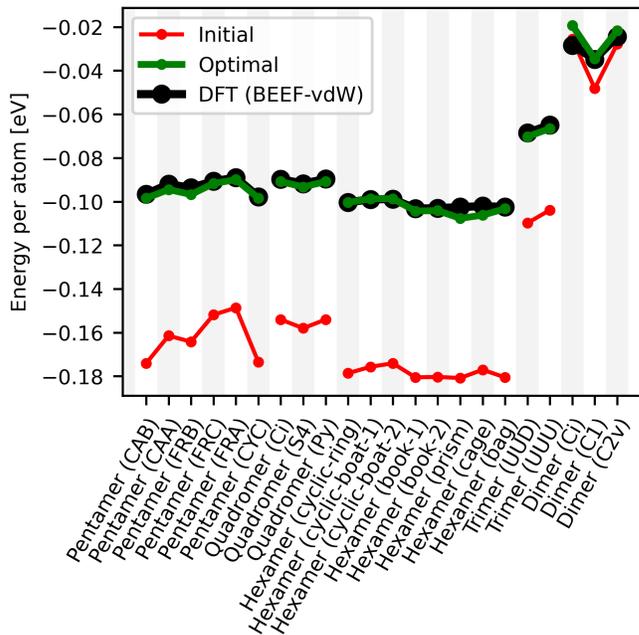


Figure 5: Energy per atom, in eV, of the initial, optimal and reference (DFT) geometries of water clusters. Agreement of the optimal geometries with those obtained from DFT calculations with the BEEF-vdW functional is within 0.01 eV per atom.

Conclusions

We have presented ChemFit, a flexible and scalable framework for defining and evaluating simulation-based objective functions in parameter optimization problems. ChemFit enables the effective application of gradient-free and black-box optimization methods to problems characterized by expensive, noisy, and heterogeneous

simulations. The key contribution of ChemFit lies in its explicit treatment of concurrency and heterogeneity. Through abstractions for independent objective-function terms and controlled allocation of computational resources, the framework allows users to efficiently exploit modern high-performance computing environments without embedding optimization logic into simulation workflows. This design makes ChemFit applicable across a broad range of scientific domains and simulation scales.

The LJ case study illustrates how optimal parameters can be found even when starting from a very different region of the parameter hyperspace with a noisy objective function, showing how ChemFit could be helpful in parameterizing novel systems and model potentials. Furthermore, a combined objective function could consist of more than one type of calculation: for instance, it could be obtained from densities (as shown in this example) along with other commonly used target properties of interest, such as the solubility, surface tension or viscosity.^{61,63,77}

The SCME parameterization example shows how structure optimization against high-level calculations can be used to obtain good agreement with the energy. This could potentially be useful for parameterizing coarse-grained models, which may have different energy scales from higher-level calculations, making it sub-optimal to fit to the energies directly.^{14,17} We anticipate that the framework could be valuable in applications that combine high-dimensional parameter spaces with increasingly complex and computationally demanding models.

Acknowledgement A.G. acknowledges a post-doctoral grant from the Icelandic Research Fund (grant no. 228615). E.O.J acknowledges project grant from the Icelandic Research Fund (grant no. 2410644). J. R. E. acknowledges funding from the University of Cambridge, the Ramon y Cajal fellowship (RYC2021-030937-I), the Spanish scientific plan and committee for research reference PID2022-136919NA-C33, and the European Research Council (ERC) under the European Union’s Horizon Europe research and innovation program (grant agreement no. 101160499). The calculations were performed using compute resources

provided by Barcelona Supercomputing Center - Centro Nacional de Supercomputación (The Spanish National Supercomputing Center) and the Icelandic Research Electronic Infrastructure (IREI). We are grateful to Magnus A. H. Christiansen for providing the DFT calculations which were used as a reference for fitting the SCME/f parameters. We thank Carlos Vega and Rohit Goswami for fruitful discussions.

Supporting Information Available

The authors confirm that the data supporting the findings of this study are available within the article and/or its supplementary materials. The supporting information contains a description of the simulation protocol for each of the examples, a plot comparing experimental densities of liquid Argon with those obtained from simulations with the optimal LJ parameters, a figure depicting the LJ parameters found in this work compared to those from the literature, and the electrostatic damping in the SCME. Snapshots in this work were created using `Solvvis2`.^{78,79}

ChemFit is a free and open-source code, available on GitHub⁸⁰ with online documentation.⁴⁰ Code for running the examples in this article are also available on GitHub.⁴¹

References

- (1) Harrison, J. A.; Schall, J. D.; Maskey, S.; Mikulski, P. T.; Knippenberg, M. T.; Morrow, B. H. Review of force fields and intermolecular potentials used in atomistic computational materials research. *Appl. Phys. Rev.* **2018**, *5*.
- (2) Müser, M. H.; Sukhomlinov, S. V.; Pastewka, L. Interatomic potentials: achievements and challenges. *Adv. Phys.: X* **2022**, *8*.
- (3) Jorgensen, W. L.; Maxwell, D. S.; Tirado-Rives, J. Development and Testing of the OPLS All-Atom Force Field on Conformational Energetics and Properties of Organic

- Liquids. *J. Am. Chem. Soc.* **1996**, *118*, 11225–11236.
- (4) Hornak, V.; Abel, R.; Okur, A.; Strockbine, B.; Roitberg, A.; Simmerling, C. Comparison of multiple Amber force fields and development of improved protein backbone parameters. *Proteins* **2006**, *65*, 712–725.
 - (5) Leontyev, I. V.; Stuchebrukhov, A. A. Electronic continuum model for molecular dynamics simulations of biological molecules. *J. Chem. Theory Comput.* **2010**, *6*, 1498–1508.
 - (6) Kirby, B. J.; Jungwirth, P. Charge scaling manifesto: A way of reconciling the inherently macroscopic and microscopic natures of molecular simulations. *J. Phys. Chem. Lett.* **2019**, *10*, 7531–7536.
 - (7) Cruces Chamorro, V.; Jungwirth, P.; Martinez-Seara, H. Building water models compatible with charge scaling molecular dynamics. *J. Phys. Chem. Lett.* **2024**, *15*, 2922–2928.
 - (8) Jorge, M.; Lue, L. The dielectric constant: Reconciling simulation and experiment. *J. Chem. Phys.* **2019**, *150*, 084108.
 - (9) Le Breton, G.; Joly, L. Molecular modeling of aqueous electrolytes at interfaces: Effects of long-range dispersion forces and of ionic charge rescaling. *J. Chem. Phys.* **2020**, *152*, 241102.
 - (10) Wikfeldt, K. T.; Batista, E. R.; Vila, F. D.; Jónsson, H. A Transferable H₂O Interaction Potential Based on a Single Center Multipole Expansion: SCME. *Phys. Chem. Chem. Phys.* **2013**, *15*, 16542–16556.
 - (11) Noid, W. G. Perspective: Coarse-grained models for biomolecular systems. *J. Chem. Phys.* **2013**, *139*.
 - (12) Brini, E.; Algaer, E. A.; Ganguly, P.; Li, C.; Rodríguez-Ropero, F.; van der Vegt, N. F. A. Systematic coarse-graining methods for soft matter simulations – a review. *Soft Matter* **2013**, *9*, 2108–2119.
 - (13) Molinero, V.; Moore, E. B. Water Modeled As an Intermediate Element between Carbon and Silicon. *J. Phys. Chem. B* **2008**, *113*, 4008–4016.
 - (14) Joseph, J. A.; Reinhardt, A.; Aguirre, A.; Chew, P. Y.; Russell, K. O.; Espinosa, J. R.; Garaizar, A.; Collepardo-Guevara, R. Physics-driven coarse-grained model for biomolecular phase separation with near-quantitative accuracy. *Nat. Comput. Sci.* **2021**, *1*, 732–743.
 - (15) Souza, P. C. T. et al. Martini 3: a general purpose force field for coarse-grained molecular dynamics. *Nat. Methods* **2021**, *18*, 382–388.
 - (16) Cao, F.; von Bülow, S.; Tesei, G.; Lindorff-Larsen, K. A coarse-grained model for disordered and multi-domain proteins. *Protein Sci.* **2024**, *33*.
 - (17) R. Tejedor, A.; Aguirre Gonzalez, A.; Maristany, M. J.; Chew, P. Y.; Russell, K.; Ramirez, J.; Espinosa, J. R.; Collepardo-Guevara, R. Chemically Informed Coarse-Graining of Electrostatic Forces in Charge-Rich Biomolecular Condensates. *ACS Cent. Sci.* **2025**, *11*, 302–321.
 - (18) Hess, T.; Vogel, C.; Maier, L.; Barcza, A.; Vieyra, H.; Schäfer-Welsen, O.; Wöllenstein, J.; Bartholomé, K. Phenomenological model for a first-order magnetocaloric material. *Int. J. Refrig.* **2020**, *109*, 128–134.
 - (19) Fedotov, A. Analysis of the adequacy and selection of phenomenological models of the elastic properties of porous powder materials. *J. Mater. Sci.* **2016**, *52*, 2964–2973.
 - (20) Kolda, T. G.; Lewis, R. M.; Torczon, V. Optimization by Direct Search: New Perspectives on Some Classical and Modern Methods. *SIAM Rev.* **2003**, *45*, 385–482.
 - (21) Wild, S. M.; Regis, R. G.; Shoemaker, C. A. ORBIT: Optimization by Radial Basis Function Interpolation in Trust-Regions. *SIAM J. Sci. Comput.* **2008**, *30*, 3197–3219.

- (22) Rios, L. M.; Sahinidis, N. V. Derivative-free optimization: a review of algorithms and comparison of software implementations. *J. Glob. Optim.* **2012**, *56*, 1247–1293.
- (23) Bäck, T.; Schwefel, H.-P. An Overview of Evolutionary Algorithms for Parameter Optimization. *Evol. Comput.* **1993**, *1*, 1–23.
- (24) Rakshit, P.; Konar, A.; Das, S. Noisy evolutionary optimization algorithms – A comprehensive survey. *Swarm Evol. Comput.* **2017**, *33*, 18–45.
- (25) Lin, T.; Zheng, Z.; Jordan, M. Gradient-free methods for deterministic and stochastic non-smooth nonconvex optimization. *Adv. Neural Inf. Process. Syst.* **2022**, *35*, 26160–26175.
- (26) Kozak, D.; Becker, S.; Doostan, A.; Tenorio, L. A stochastic subspace approach to gradient-free optimization in high dimensions. *Comput. Optim. Appl.* **2021**, *79*, 339–368.
- (27) Shahriari, B.; Swersky, K.; Wang, Z.; Adams, R. P.; de Freitas, N. Taking the Human Out of the Loop: A Review of Bayesian Optimization. *Proc. IEEE* **2016**, *104*, 148–175.
- (28) Frazier, P. I. *Recent Advances in Optimization and Modeling of Contemporary Problems*; INFORMS, 2018; pp 255–278.
- (29) Wang, X.; Jin, Y.; Schmitt, S.; Olhofer, M. Recent Advances in Bayesian Optimization. *ACM Comput. Surv.* **2023**, *55*, 1–36.
- (30) Binois, M.; Wycoff, N. A Survey on High-dimensional Gaussian Process Modeling with Application to Bayesian Optimization. *ACM Trans. Evol. Learn. Optim.* **2022**, *2*, 1–26.
- (31) Goswami, R.; Jónsson, H. Adaptive Pruning for Increased Robustness and Reduced Computational Overhead in Gaussian Process Accelerated Saddle Point Searches. *ChemPhysChem* **2025**,
- (32) Snoek, J.; Larochelle, H.; Adams, R. P. Practical bayesian optimization of machine learning algorithms. *Adv. Neural Inf. Process. Syst.* **2012**, *25*.
- (33) Jones, D. R.; Schonlau, M.; Welch, W. J. Efficient Global Optimization of Expensive Black-Box Functions. *J. Glob. Optim.* **1998**, *13*, 455–492.
- (34) Bischl, B.; Binder, M.; Lang, M.; Pielok, T.; Richter, J.; Coors, S.; Thomas, J.; Ullmann, T.; Becker, M.; Boulesteix, A.; Deng, D.; Lindauer, M. Hyperparameter optimization: Foundations, algorithms, best practices, and open challenges. *Data Min. Knowl. Discov.* **2023**, *13*.
- (35) Turner, R.; Eriksson, D.; McCourt, M.; Kili, J.; Laaksonen, E.; Xu, Z.; Guyon, I. Bayesian Optimization is Superior to Random Search for Machine Learning Hyperparameter Tuning: Analysis of the Black-Box Optimization Challenge 2020. Proceedings of the NeurIPS 2020 Competition and Demonstration Track. 2021; pp 3–26.
- (36) Terayama, K.; Sumita, M.; Tamura, R.; Tsuda, K. Black-Box Optimization for Automated Discovery. *Acc. Chem. Res.* **2021**, *54*, 1334–1346.
- (37) Foster, A.; Jankowiak, M.; Bingham, E.; Horsfall, P.; Teh, Y. W.; Rainforth, T.; Goodman, N. Variational Bayesian optimal experimental design. *Adv. Neural Inf. Process. Syst.* **2019**, *32*.
- (38) Li, Y.; Shen, Y.; Zhang, W.; Chen, Y.; Jiang, H.; Liu, M.; Jiang, J.; Gao, J.; Wu, W.; Yang, Z.; Zhang, C.; Cui, B. OpenBox: A Generalized Black-box Optimization Service. Proceedings of the 27th ACM SIGKDD Conference on Knowledge Discovery & Data Mining. 2021; pp 3209–3219.
- (39) Hjorth Larsen, A. et al. The Atomic Simulation Environment—a Python Library for Working with Atoms. *J. Phys.: Condens. Matter* **2017**, *29*, 273002.
- (40) Sallermann, M. ChemFit Documentation. <https://chemfit.readthedocs.io/en/latest/>, 2026; Online documentation. Accessed 2026-03-08.

- (41) Sallermann, M. ChemFit Examples: Example applications for the ChemFit framework. <https://github.com/MSallermann/chemfit-examples>, 2026; GitHub repository. Accessed 2026-03-08.
- (42) Thompson, A. P.; Aktulga, H. M.; Berger, R.; Bolintineanu, D. S.; Brown, W. M.; Crozier, P. S.; in 't Veld, P. J.; Kohlmeyer, A.; Moore, S. G.; Nguyen, T. D.; Shan, R.; Stevens, M. J.; Tranchida, J.; Trott, C.; Plimpton, S. J. LAMMPS - a flexible simulation tool for particle-based materials modeling at the atomic, meso, and continuum scales. *Comput. Phys. Commun.* **2022**, *271*, 108171.
- (43) Abraham, M. J.; Murtola, T.; Schulz, R.; Páll, S.; Smith, J. C.; Hess, B.; Lindahl, E. GROMACS: High performance molecular simulations through multi-level parallelism from laptops to supercomputers. *SoftwareX* **2015**, *1–2*, 19–25.
- (44) Kresse, G.; Furthmüller, J. Efficient Iterative Schemes for Ab Initio Total-Energy Calculations Using a Plane-Wave Basis Set. *Phys. Rev. B* **1996**, *54*, 11169–11186.
- (45) Spiteri, R. J.; Klenk, K. *Extreme-Scale Computing*; Springer Nature Switzerland, 2025; pp 177–186.
- (46) Raffenetti, K. et al. Why is MPI so slow?: analyzing the fundamental limits in implementing MPI-3.1. Proceedings of the International Conference for High Performance Computing, Networking, Storage and Analysis. 2017; pp 1–12.
- (47) Rocklin, M.; others Dask: Parallel computation with blocked algorithms and task scheduling. SciPy. 2015; pp 126–132.
- (48) Lennard-Jones, J. E. Cohesion. *Proceedings of the Physical Society* **1931**, *43*, 461–482.
- (49) London, F. Zur theorie und systematik der molekularkräfte. *Zeitschrift für Physik* **1930**, *63*, 245–279.
- (50) Jones, J. E. On the determination of molecular fields. —II. From the equation of state of a gas. *Proceedings of the Royal Society of London. Series A, Containing Papers of a Mathematical and Physical Character* **1924**, *106*, 463–477.
- (51) Kulakova, L.; Arampatzis, G.; Angelikopoulos, P.; Hadjidoukas, P.; Papadimitriou, C.; Koumoutsakos, P. Data driven inference for the repulsive exponent of the Lennard-Jones potential in molecular dynamics simulations. *Sci. Rep.* **2017**, *7*.
- (52) van der Hoef, M. A.; Madden, P. A. Three-body dispersion contributions to the thermodynamic properties and effective pair interactions in liquid argon. *J. Chem. Phys.* **1999**, *111*, 1520–1526.
- (53) Wang, X.; Ramírez-Hinestrosa, S.; Dobnikar, J.; Frenkel, D. The Lennard-Jones potential: when (not) to use it. *Phys. Chem. Chem. Phys.* **2020**, *22*, 10624–10633.
- (54) Goujon, F.; Malfreyt, P.; Tildesley, D. J. The gas-liquid surface tension of argon: A reconciliation between experiment and simulation. *J. Chem. Phys.* **2014**, *140*.
- (55) Streett, W. B.; Staveley, L. A. K. Experimental Study of the Equation of State of Liquid Argon. *J. Chem. Phys.* **1969**, *50*, 2302–2307.
- (56) Rahman, A. Correlations in the Motion of Atoms in Liquid Argon. *Phys. Rev.* **1964**, *136*, A405–A411.
- (57) Barker, J.; Fisher, R.; Watts, R. Liquid argon: Monte carlo and molecular dynamics calculations. *Mol. Phys.* **1971**, *21*, 657–673.
- (58) Rowley, L.; Nicholson, D.; Parsonage, N. Monte Carlo grand canonical ensemble calculation in a gas-liquid transition region for 12-6 Argon. *J. Comput. Phys.* **1975**, *17*, 401–414.
- (59) White, J. A. Lennard-Jones as a model for argon and test of extended renormalization group calculations. *J. Chem. Phys.* **1999**, *111*, 9352–9356.

- (60) Stephan, S.; Thol, M.; Vrabec, J.; Hasse, H. Thermophysical Properties of the Lennard-Jones Fluid: Database and Data Assessment. *J. Chem. Inf. Model* **2019**, *59*, 4248–4265.
- (61) Zeron, I. M.; Abascal, J. L. F.; Vega, C. A force field of Li^+ , Na^+ , K^+ , Mg^{2+} , Ca^{2+} , Cl^- , and SO_4^{2-} in aqueous solution based on the TIP4P/2005 water model and scaled charges for the ions. *J. Chem. Phys.* *151*, 134504.
- (62) Zhang, W.; Van Duin, A. C. Second-generation ReaxFF water force field: improvements in the description of water density and OH-anion diffusion. *J. Phys. Chem. B* **2017**, *121*, 6021–6032.
- (63) Méndez-Bermúdez, J. G.; Guillén-Escamilla, I.; Méndez-Maldonado, G. A.; Alva-Tamayo, J. A. D. Argon force field revisited: a molecular dynamic study. *J. Phys. Commun.* **2022**, *6*, 041002.
- (64) Jónsson, E. O.; Dohn, A. O.; Jonsson, H. Polarizable Embedding with a Transferable H_2O Potential Function I: Formulation and Tests on Dimer. *J. Chem. Theory Comput.* **2019**, *15*, 6562–6577.
- (65) Dohn, A. O.; Jónsson, E. O.; Jónsson, H. Polarizable Embedding with a Transferable H_2O Potential Function II: Application to $(\text{H}_2\text{O})_N$ Clusters and Liquid Water. *J. Chem. Theory Comput.* **2019**, *15*, 6578–6587.
- (66) Jónsson, E. Ö.; Rasti, S.; Galynska, M.; Meyer, J.; Jónsson, H. Transferable Potential Function for Flexible H_2O Molecules Based on the Single-Center Multipole Expansion. *J. Chem. Theory Comput.* **2022**, *18*, 7528–7543.
- (67) Myneni, H.; Jónsson, E. Ö.; Jónsson, H.; Dohn, A. O. Polarizable force field for acetonitrile based on the single-center multipole expansion. *The Journal of Physical Chemistry B* **2022**, *126*, 9339–9348.
- (68) Lundgaard, K. T.; Wellendorff, J.; Voss, J.; Jacobsen, K. W.; Bligaard, T. mBEEF-vdW: Robust Fitting of Error Estimation Density Functionals. *Phys. Rev. B* **2016**, *93*, 235162.
- (69) Kim, J.; Kim, K. S. Structures, binding energies, and spectra of isoenergetic water hexamer clusters: Extensive ab initio studies. *J. Chem. Phys.* **1998**, *109*, 5886–5895.
- (70) Petty, B. T.; Fowler, V. R.; Ryu, A.; Glick, C. S.; Rock, C. A.; Wang, Q.; Tschumper, G. S.; Shields, G. C. Reliable Structures and Electronic Energies of Small Water Clusters Using Density Functional and Local Correlation Coupled Cluster Model Chemistries. *J. Phys. Chem. A* **2025**, *129*, 9291–9302.
- (71) Partridge, H.; Schwenke, D. W. The Determination of an Accurate Isotope Dependent Potential Energy Surface for Water from Extensive Ab Initio Calculations and Experimental Data. *J. Chem. Phys.* **1997**, *106*, 4618–4639.
- (72) Stone, A. J. Electrostatic Damping Functions and the Penetration Energy. *J. Phys. Chem. A* **2011**, *115*, 7017–7027.
- (73) Tang, K. T.; Toennies, J. P. An Improved Simple Model for the van Der Waals Potential Based on Universal Damping Functions for the Dispersion Coefficients. *J. Chem. Phys.* **1984**, *80*, 3726–3741.
- (74) Hettema, H.; Wormer, P. E. S.; Jørgensen, P.; Jensen, H. J. Aa.; Helgaker, T. Frequency-dependent Polarizabilities of O_2 and van Der Waals Coefficients of Dimers Containing O_2 . *J. Chem. Phys.* **1994**, *100*, 1297–1302.
- (75) Kabsch, W. A solution for the best rotation to relate two sets of vectors. *Acta Crystallogr. A* **1976**, *32*, 922–923.
- (76) Kabsch, W. A discussion of the solution for the best rotation to relate two sets of vectors. *Acta Crystallogr. A* **1978**, *34*, 827–828.
- (77) Goswami, A.; Blazquez, S.; Fernández-Sedano, L.; Noya, E. G.; Jónsson, H.; Troncoso, J.; Vega, C. Viscosity as a Smoking Gun for Complex Formation in Solution: Fe^{2+} and Mg^{2+} Chlorides as Examples. 2026.
- (78) Sallermann, M. Solvis2. <https://github.com/amro-tools/Solvis2>, 2026; GitHub repository. Accessed 2026-03-08.

- (79) Goswami, A. Solvis. <https://github.com/amritagos/solvis>, 2026; GitHub repository. Accessed 2026-03-08.
- (80) Sallermann, M. ChemFit: Framework for hyper-concurrent chemical objective functions. <https://github.com/MSallermann/chemfit>, 2026; GitHub repository. Accessed 2026-03-08.

Supporting Information

ChemFit: A concurrent framework for model parametrization

Moritz Sallermann, Amrita Goswami, Hannes Jónsson, Elvar Ö. Jónsson, Jorge R. Espinosa

S1 Simulation protocol	16
S1.1 Lennard-Jones example	16
S2 LJ parameterization results	16
S3 SCME electrostatic damping	17
References	18

S1 Simulation protocol

S1.1 Lennard-Jones example

We used 1000 Argon atoms, with a Nosé–Hoover thermostat^{S1} with a coupling constant of 100 fs, as well as the Nosé–Hoover barostat^{S2} with a coupling constant of 1000 fs. For the initial box, we used a cube with a side length of

$$L_{\text{init}} = 2\sigma (n_{\text{atoms}})^{1/3}, \quad (\text{S1})$$

in which we let LAMMPS randomly place atoms while maintaining a minimum distance of

$$\Delta_{\text{min}} = 1.2\sigma \quad (\text{S2})$$

between atoms. We use the "truncated and shifted" version of the LJ potential (lj/cut pairstyle in LAMMPS) with a cutoff radius of

$$r_c = 5\sigma. \quad (\text{S3})$$

For each data point, the system was equilibrated for 2 ps in the NVT ensemble maintaining the initial box size L_{init} and at the experimental temperature. Then, the system was equilibrated for 20 ps in the NPT ensemble at the experimental temperature and pressure. Lastly, the "production" run lasted another 20 ps and the density was computed by averaging the instantaneous densities every 2 ps. The timestep for all runs was 2 fs.

S2 LJ parameterization results

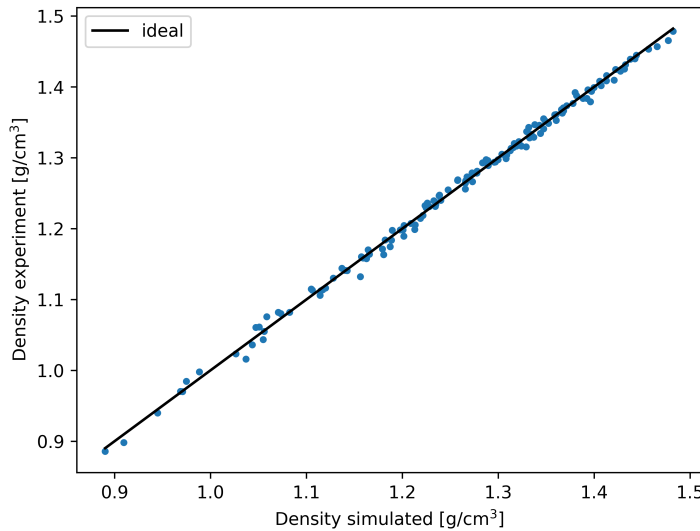


Figure S1: Density from the reference experiments^{S3} versus the density obtained from simulations using optimal parameters. The solid black line denotes the ideal scenario in which the simulated densities are identical to the reference densities.

Fig. S1 visually depicts the agreement of densities obtained from simulations of the LJ potential, using the optimal parameters, with the reference densities from experiments.^{S3}

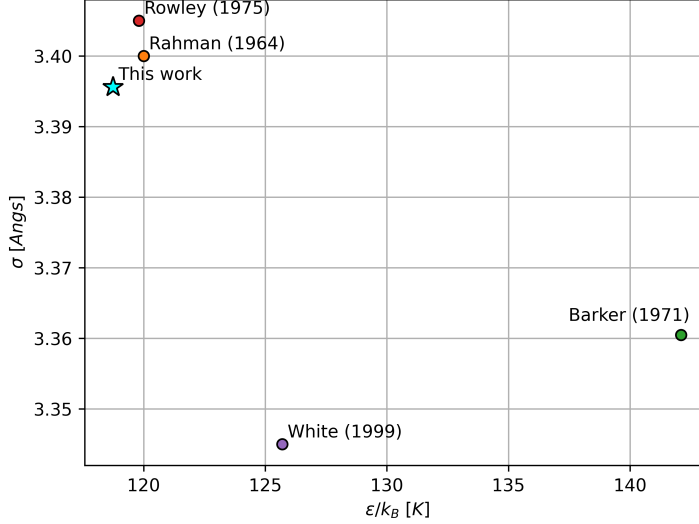


Figure S2: The size parameter, σ (in Å), versus the binding energy, ϵ (in k_B), for the optimal parameters obtained in this work and those from the literature.^{S4–S7}

Fig. S2 shows the optimal parameters (cyan star) obtained in this work, compared to those from the literature^{S4–S7} in the σ - ϵ hyperspace.

S3 SCME electrostatic damping

In general the electric field V^{ij} at a position r_i due to a moment M at a position r_j is given by an equation of the form

$$V_\alpha^{ij} = T_{\alpha\beta\dots\gamma}^{ij} M_{\beta\dots\gamma}, \quad (\text{S4})$$

where the notation $\beta\dots\gamma$ means there are as many indices as the rank of the moment (i.e., two for a dipole moment, three for a quadrupole moment etc.) and $T_{\alpha\beta\dots\gamma}^{ij}$ is a Coulomb tensor of appropriate rank. The Coulomb tensors can be defined recursively as

$$T^{ij} = \frac{1}{r} \lambda_0(r) \quad (\text{S5})$$

$$T_\alpha^{ij} = \nabla_\alpha T^{ij} = -\frac{r_\alpha}{r^3} \lambda_1(r) \quad (\text{S6})$$

$$T_{\alpha\beta}^{ij} = \nabla_\beta T_\alpha^{ij} = 3 \frac{r_\alpha r_\beta}{r^5} \lambda_2(r) - \frac{\delta_{\alpha\beta}}{r^3} \lambda_1(r) \quad (\text{S7})$$

and so on.

The $\lambda_n(r)$ damping functions are due to Stone^{S8}:

$$\lambda_n(r) = \lambda_n(S(r)) = \text{erf}(S) - \frac{2}{\sqrt{\pi}} e^{-S^2} \left(\sum_{i=1}^n \frac{2^{i-1} S^{2i-1}}{(2i-1)!!} \right), \quad (\text{S8})$$

where

$$S = \frac{r}{\tau_E},$$

and $x!! := 1 \cdot 3 \cdot \dots \cdot (x-2) \cdot x$ denotes the double factorial.

References

- S1. Evans, D. J.; Holian, B. L. The Nose-Hoover thermostat. *J. Chem. Phys.* **1985**, *83*, 4069–4074.
- S2. Shinoda, W.; Shiga, M.; Mikami, M. Rapid estimation of elastic constants by molecular dynamics simulation under constant stress. *Phys. Rev. B* **2004**, *69*, 134103.
- S3. Strett, W. B.; Staveley, L. A. K. Experimental Study of the Equation of State of Liquid Argon. *J. Chem. Phys.* **1969**, *50*, 2302–2307.
- S4. Rahman, A. Correlations in the Motion of Atoms in Liquid Argon. *Phys. Rev.* **1964**, *136*, A405–A411.
- S5. Rowley, L.; Nicholson, D.; Parsonage, N. Monte Carlo grand canonical ensemble calculation in a gas-liquid transition region for 12-6 Argon. *J. Comput. Phys.* **1975**, *17*, 401–414.
- S6. White, J. A. Lennard-Jones as a model for argon and test of extended renormalization group calculations. *J. Chem. Phys.* **1999**, *111*, 9352–9356.
- S7. Barker, J.; Fisher, R.; Watts, R. Liquid argon: Monte carlo and molecular dynamics calculations. *Mol. Phys.* **1971**, *21*, 657–673.
- S8. Stone, A. J. Electrostatic Damping Functions and the Penetration Energy. *J. Phys. Chem. A* **2011**, *115*, 7017–7027.